Optical and Quantum Electronics (2023) 55:507
https://doi.org/10.1007/s11082-023-04788-8

Refractive index based optically transparent biosensor device design for early detection of coronavirus

A. M. Balamurugan[1] · Tarunnum Parvin[2] · Kasim Abdul Jabar Alsalem[3] · Sobhy M. Ibrahim[4]

Received: 25 January 2023 / Accepted: 21 March 2023 / Published online: 8 April 2023

Abstract

For the quick detection of the new Coronavirus (COVID-19), a highly sensitive D-shaped gold-coated surface Plasmon resonance (SPR) biosensor is presented. The COVID-19 virus may be quickly and accurately identified using the SPR-based biosensor, which is essential for halting the spread of this excruciating epidemic. The suggested biosensor is used for detection of the IBV i.e. infectious bronchitis viruses contaminated cell that belongs to the family of COVID-19 having a refractive index of $-0.96, -0.97, -0.98, -0.99, -1$ that is observed with the change in EID concentration. Some important optical parameter variations are examined in the investigation process. Multiphysics version 5.3 with the Finite element method is used for the proposed biosensor. The proposed sensor depicts maximum wavelength sensitivity of 40,141.76 nm/RIU. Some other parameters such as confinement loss, crosstalk, and insertion loss are also analyzed for the proposed sensor. The reported minimum insertion loss for the refractive index (RI) -1 is 2.9 dB. Simple design, good sensitivity, and lower value of losses make the proposed sensor proficient for the detection of infectious bronchitis viruses belonging to COVID-19.

✉ Tarunnum Parvin
tarannump.ph21.ec@nitp.ac.in; tarannumparveen09@gmail.com

A. M. Balamurugan
balamurugan0902@gmail.com

Kasim Abdul Jabar Alsalem
qasim.abd@kunoozu.edu.iq

Sobhy M. Ibrahim
syakout@ksu.edu.sa

[1] Department of ECE, St.Joseph's College of Engineering, Chennai 600 119, India

[2] Department of Electronics and Communication, N.I.T Patna, Patna, India

[3] Department of Medical Instrumentation Engineering Techniques, Al-Kunooze University College, Basra, Iraq

[4] Department of Biochemistry, College of Science, King Saud University, P.O. Box 2455, Riyadh 11451, Saudi Arabia

Graphical abstract

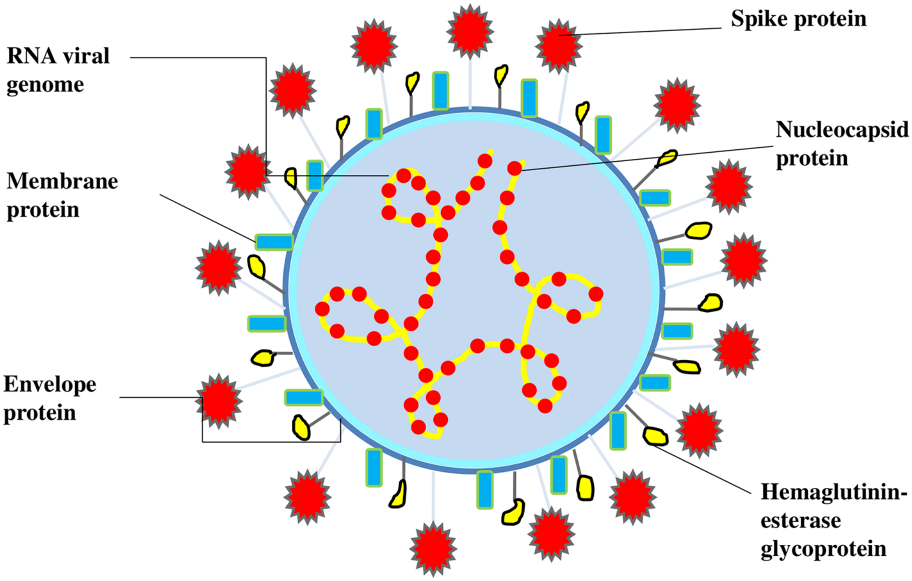

Keywords Coronavirus detection · D-shaped biosensor · Optically transparent device · Refractive index sensor · Surface plasmon resonance

1 Introduction

In December 2019, the novel coronavirus, named COVID-19 by WHO, was first found in Wuhan city of China. These virus spreads worldwide and disrupted the regular life and economy of the entire world. Due to this out of 160 million positive cases, 3.25 million people deceased. WHO has confirmed the epidemic of transferable viruses in humans as a global pandemic. SARS-CoV-2, which spreads through breathing, direct contact with abiotic surfaces and aerosol particles, and aerosol particles themselves, is the coronavirus that causes the disease (COVID-19). Evidence of transmission of the virus is also observed through fecal. Symptoms of SARS-CoV-2 are high fever, throat infection, body ache, loss of taste and smell, headache, and diarrhea. It is asymptomatic in behavior in its early stage for a few patients who act as a silent killer as it damages vital organs within a shorter period. Hence there is an urgent requirement for a device that can detect the virus within a shorter period at an early stage with a precise result in a cost-effective manner. SARS-CoV-2 is a single RNA virus that contains four substantial proteins namely spike(s) glycoprotein, membrane (M), envelope (E), and nucleocapsid (N) protein (Astuti 2020). When the spike protein of the virus activates, it can damage the brain, heart, and kidneys of humans (Gheblawi et al. 2020). In this regard, WHO has insisted the scientific community perform a large number of investigations to control the spread of coronavirus besides, rapid diagnostic testing is essential in making a swift decision for the treatment of the patient. Some tests are available to detect the existence of coronavirus in the human body namely RT_PCR, real-time RT-LAMP, and reverse transcription loop-mediated isothermal amplification (RT-PCR) (Shirato et al. 2018; Yan et al. 2020). However

SARS-CoV-2 antigen fast test kit that is used for the detection of COVID-19 is less sensitive in comparison to RT-PCR (Mak et al. 2020; Krüttgen et al. 2021) and results are confirmed after CT-scan chest computed tomography (Korevaar et al. 2020; Chen et al. 2020). Biosensors had already proved their potential for deadly diseases like cancer, tuberculosis, and dengue. As biosensors exhibit unique features, are simple in design, and are cost-effective, they could be a useful tool in screening "COVID-19 ". It also holds massive prospects for reliable and affordable diagnostics, especially for developing countries where infrastructure and resources are limited. SPR is a paramount conventional technique that is consistent in practical application over the last three decades for the detection of biomolecular interactions either clinical or for research purposes The SPR is a bio-analytical process for real-time detection of ligand-analyte binding onto the sensing area. Nowadays various industries are developing SPR-based sensors like compact SPR biosensors, localized SPR, and optical sensing SPR biosensors. Moreover, photonic crystal fiber (PCF) is very small and lightweight, which ensures the compactness and miniaturization of the biosensor (Islam et al. 2018; Qin et al. 2014).

However, the operating principles of these biosensors are similar. Cui et al. (2010) proposed an SPR-based system to detect SARS-CoV. The proposed model consists of two types. In the type-1 model, the monoclonal antibodies were immobilized to the biosensor surface of SARS-CoV and in the type-2 model, the experiment involved Protein A in the biosensor device. Due to the addition of Protein A, the free degree of the antibodies is elevated and it increases the distance between the antibodies and the biosensor surface (Cui et al. 2010). Ahmadivand et al. (2020) designed an SPR biosensor with gold nanoparticles (AuNPs) and a monoclonal antibody immobilized on the sensing layer to recognize the S1 protein of SARS-CoV2 (Ahmadivand et al. 2020).

Das et al. (2020) proposed a sandwich plasmonic biosensor in which a gold (Au) Nanosheet is deposited as a sensing layer along with an S protein antibody (Ab) (Das et al. 2020). Djaileb et al. (2020) presented an SPR biosensor in which peptide monolayer, 3 mercapto propionic-Leu-His–Asp–Leu– His–Asp–COOH were fabricated on the sensing layer to recognize N antibodies specific for SARS-CoV2 in human serum. The developed biosensor showed very high selectivity towards the N protein also during the SPR biosensor was injected with various kinds of antigens such as anti-prostate-specific antigens (Djaileb et al. 2020). In Akib et al. (2021) suggested a highly sensitive multilayer graphene-based SPR biosensor for the fast detection of the COVID-19. The designed model is based on total internal reflection for real-time detecting ligand analyte immobilization in the sensing area. A promising photonic crystal fibre sensor based on the Sagnac interferometer to identify malignant cells was proposed by Mollah et al. (2020). A revolutionary SPR-based fuel adulteration Photonic biosensor was created by Hossain et al. (2023). Tanvir et al. (2023) Hollow-Core's Anti-Resonant Fiber for gas detection was proposed in 2023. In Sorathiya et al. 2022 developed a far-infrared metasurface polarizer with an ultra-thin, broad bandwidth of 1–15 THz.

In this study, a very effective sensor with a straightforward design, good sensitivity, and low losses has been suggested for the detection of COVID-19-related infectious bronchitis viruses (IBVs).

2 Methodology

The plasmonic biosensor is significantly influenced by plasmonic material. Currently, lots of plasmonic materials are available. Among them, gold, silver, and aluminum are more popular and efficient. Silver (Ag) provides enhanced sensitivity with a higher resonance peak but there is an oxidation problem in an aqueous humid environment. Although this difficulty can be removed by using a graphene layer complexity arises in fabrication. Also, it deteriorates in a short time. The same issues arise with aluminum and copper. Gold is the most appropriate plasmonic material. Since it has high biocompatibility with less oxidation in an aqueous and humid environment (Mollah et al. 2019) and also compromises high resonance shift and chemical stability. In the proposed SPR sensor we have used gold as a plasmonic material due to its efficient characteristics. SPR biosensors can be classified as internally metal coated and externally metal-coated (Shafkat 2020). In the internal sensing approach, plasmonic materials are coated inside the photonic sensor while in the external sensing approach, the material is deposited in the external area (Momota and Hasan 2018). The proposed D-shaped PCF-SPR biosensor constitutes an external sensing method in which the analyte is placed on the surface to alleviate fabrication complexity and make the SPR biosensor practically possible. Also, the core region of D-shaped PCF is closer to plasmonic material which raises the interaction between an analyte and a metal layer. As an outcome, the sensing performance of the biosensor is enhanced. In our proposed design whole curvature of D-type PCF contains an apple amount of analytes that increases sensing performance, and provides more stability and robustness. Its lattice configuration, bounded in the core area contains two elliptical air holes and one rectangular air hole, where elliptical air holes of radius 0.2 μm and 1.8 μm and rectangular air holes height 6 μm and width 0.5 μm. The complete mesh consists of 7752 domain elements and 925 boundary elements. A finer mesh produces more accurate result**s** that are why finer meshing has been done here. Although a PCF bio-sensor relies on surface Plasmon event that occurs on the border of Metal and analyte, perfection is not as important due to air gaps. Silica serves as the background component. PML is fixed in the outer boundary region to absorb the scattering energy giving more accuracy in computation. Figure 1a shows the cross-sectional view and Fig. 1b exhibits the fine meshing to detect coronavirus. The accuracy of the finite element approach is highly correlated with mesh size. The outcome is more accurate the smaller the size. We used a tiny mesh for their computer simulation because of this. A conceptual diagram of (a) the test design, (b) the coronavirus structure, and (c) the free electron motions at the gold/analyte layer interface are shown in Fig. 2.

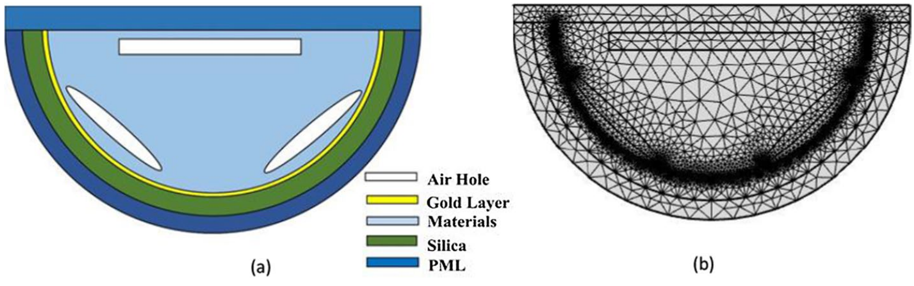

Fig. 1 Cross-sectional views of the proposed corona sensor in (**a**) and the suggested structure's fine meshing in (**b**)

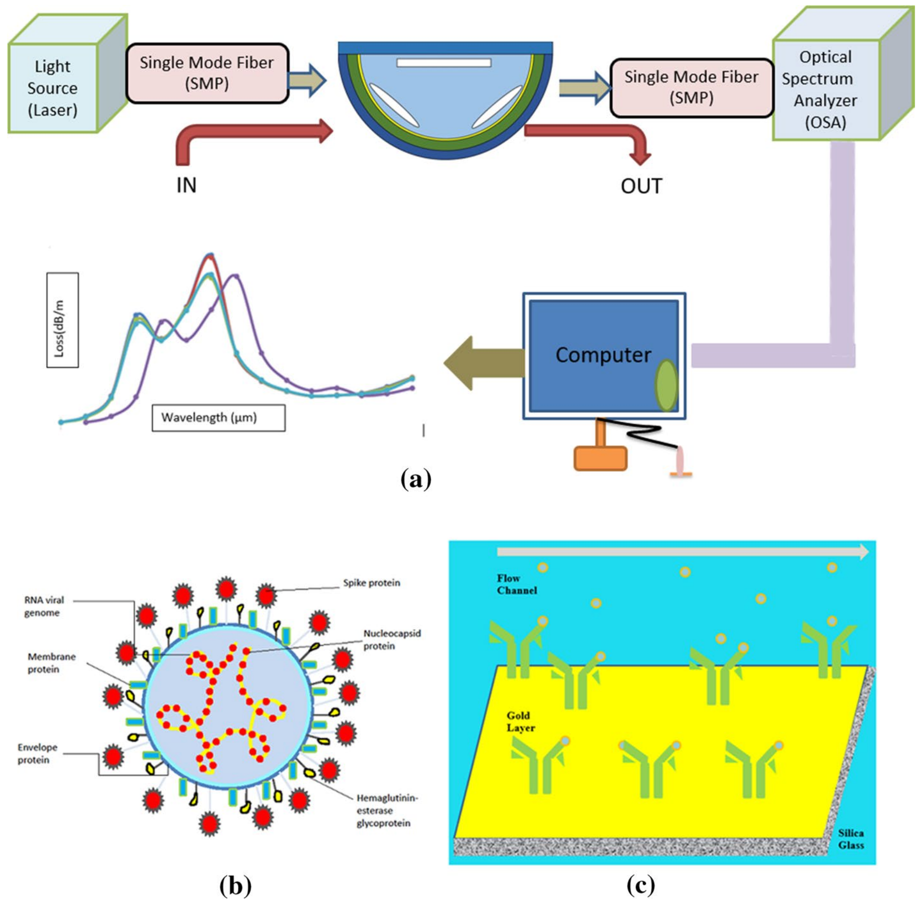

Fig. 2 Conceptual diagram of **a** the test design, **b** the coronavirus structure, and **c** the free electron motions at the gold/analyte layer interface

3 Numerical analysis

Through the process of photoluminescence intensity, an investigation of the refractive index of different coronavirus is done. The numerical result shows that the coronavirus RI is negative. Also IBV i.e. infectious bronchitis viruses that belong to the family of COVID-19 are showing a refractive index of different natures. However, variation in refractive index is studied by changing EID concentration.

For the proposed biosensor pure silica is used as the background material of the PCF. The refractive index of silica is calculated by the following Sellmeier Eq. (1) (Yang et al. 2017; Vigneswaran et al. 2018; Mamtaz et al. 2020).

$$n^2 - 1 = \sum_{x}^{3} \frac{A_p * \lambda^2}{\lambda^2 - \lambda_p^2} \tag{1}$$

Table 1 Description of different parameters of Sellimier equation

Parameter (A_p)	Values	Wavelength (λ_p)	Values
A_1	0.69616630	λ_1	0.06840430
A_2	0.40794260	λ_2	0.11624140
A_3	0.89747940	λ_3	9.8961610

Table 2 Description of different parameters of Drude–Lorentz model

Parameter	Description	Values
ε_∞	Permittivity in high frequency	5.9673
ω	Angular frequency of transmitting light	–
ω_D	Plasma frequency (THz)	2113.6*2π
γ_D	Damping frequency (THz)	$15.92 * 2\pi$
Δε	Weighting factor	1.09
Ω_L	Frequency of the Lorentz oscillator (THz)	$650.07 * 2\pi$
Γ_L	Spectral width of the Lorentz oscillator (THz)	$104.86 * 2\pi$
	Refractive index (RI) of air	1

In the following expression (1), n is the symbolization of the index of refraction for specified wavelength λ (μm). Table 1 exhibits the different parameters of the Sellimier equation. The permittivity of the gold is calculated by the Drude–Lorentz model (Hossain et al. 2023; Liu et al. 2016; Zakaria et al. 2022).

$$\varepsilon_m = \varepsilon_\infty - \frac{\omega_D^2}{\omega(\omega - j\gamma_D)} - \frac{\Delta_\varepsilon.\Omega_L^2}{\left(\omega^2 - \Omega_L^2\right) - j\Gamma_L\omega} \tag{2}$$

Table 2 exhibits different parameters of the Drude–Lorentz model. Moreover, CL is a key parameter for the biosensor and may be calculated as (Mollah et al. 2020; Vigneswaran et al. 2021; Paul et al. 2020).

$$L_C = \frac{40\pi I_m(n_{eff})10^6}{\lambda ln(10)}(\mathrm{dB/m}) \tag{3}$$

In the given Eq. (3), $I_m\left(n_{eff}\right)$ represents the imaginary section of the effective RI, and the CL is represented in decibels per meter (dB/m).

However, the displacement of the transmittance curve's peak at a certain wavelength for the overall variation of the RI allows for the evaluation of the developed sensor's WS. Table 3 exhibits the RI of corona virus for different EID concentrations. The wavelength sensitivity (Ahmed et al. 2019; Ayyanar et al. 2018), and (Sharan et al. 2014) can be defined in Eq. (4).

$$S_w\left(\frac{nm}{RIU}\right) = \frac{\Delta\lambda_p}{\Delta n} \tag{4}$$

Here, λ_p defines the change of peak wavelength and Δn defines the variation of the RI ofCOVID family cells. The difference in resolution of the suggested structure makes it

Table 3 Description of RI of coronaviruses

Class of viruses	RI		References
	0.01 [EID-Concentration]	1000 [EID-Concentration]	
H5N1	−0.752147	−0.78266	Kuppuswamy et al. (2020)
H5N2	−0.726881	−0.75739	Kuppuswamy et al. (2020)
H9N2	−0.717555	−0.74807	Kuppuswamy et al. (2020)
H4N6	−0.74535	−0.77586	Kuppuswamy et al. (2020)
FAdV	−0.714207	−0.74472	Kuppuswamy et al. (2020)
IBV (COVID-19 Group)	−0.967251	−0.999998	Kuppuswamy et al. (2020)

simple to identify any change in the RI of the biosamples. So, Eq. (5) can be used to assess the suggested model's resolution (Liu et al. 2020).

$$RI(RIU) = \frac{\Delta n \times \Delta \lambda_{min}}{\Delta \lambda_{peak}} \tag{5}$$

Here Δn is the difference between RI, $\Delta \lambda_{min}$ and $\Delta \lambda_{peak}$ are respectively for the minimum and peak wavelength differences.

The AS of the proposed corona sensor can be evaluated by given Eq. (6) shown below (Zakaria et al. 2022; Liu et al. 2020).

$$S_a\left(RIU^{-1}\right) = -\frac{1}{\propto_c} \times \frac{\Delta \alpha_c}{\Delta n} \tag{6}$$

Here, α_c corresponds to CL of the particular bio-samples, and n describes the loss difference and RI difference between corona refractive index respectively.

The CT is a crucial measurement to characterize the quality of the SPR biosensor, which determines the effect of unwanted polarization modes. CT is developed by Beer-Lambert laws (Li et al. 2017). According to the given law, the CT is a function of the length of the fiber and it can be defined as a given expression (7).

$$CT = 20lg\{exp[\left(\propto_2 - \propto_1\right)L\} \tag{7}$$

Here α_1, α_2, represent the loss of x- and y-polarization and L is the fiber length, respectively.

One of the most important considerations while examining the fiber-optic equipment is the IL (Guo et al. 2018).

$$IL[dB] = \text{Insertion Loss}[dB] = -10log_{10}\left(\frac{P_{out}}{P_{in}}\right) \tag{8}$$

In the above expression (8), P_{out} and P_{in} are, for polarised light directed in a particular direction, the input and output power, respectively.

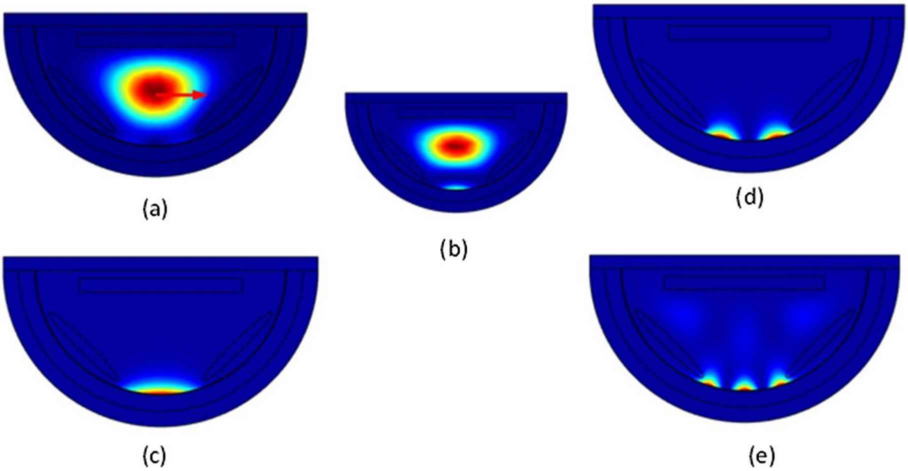

Fig. 3 Basic mode intensity distribution of the sensor in (**a**) Core (**b**) Coupling (**c**) 1st, (**d**) 2nd, and (**e**) 3rd SPP modes

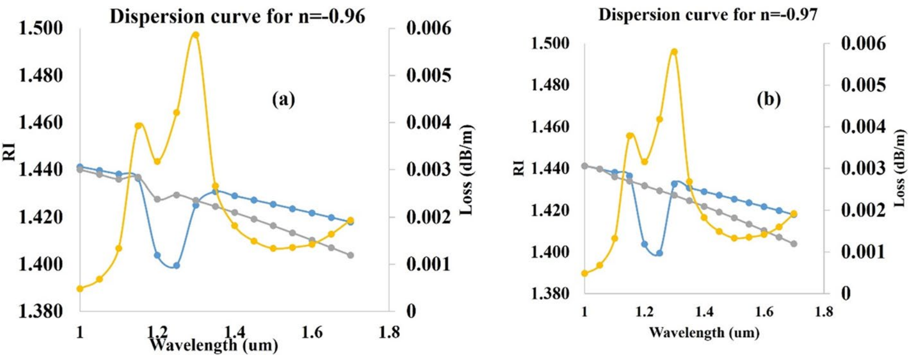

Fig. 4 Dispersion Curve for the proposed biosensor for **a** n = −0.96 and **b** n = −0.97

4 Results and analysis

Core, coupling, and SPP modes make up the mode field distributions that can be acquired from the suggested sensor. These modes are highlighted in Fig. 3. The core mode can be achieved when the light passes through the center core of the proposed sensor design. At the time of hitting the light at the gold layer, the SPP mode can be obtained. At the intersecting point of the core and SPP mode, the coupling mode can be shown. Moreover, the loss value becomes high at the intersecting point. That is also referred to as the loss peak. The intersection of core and SPP mode and the corresponding loss curve has been exhibited in Fig. 4.

The relationship between the core-guided mode's loss curve and dispersion and the plasmon mode is depicted in Fig. 4. High energy losses of the core mode linked to the plasmon are shown by the peaks in the loss curve marked by the yellow line. The core and SPP modes couple to one another at wavelengths of 1.15 μm and 1.3 μm because their

RIs are nearly identical. Since the intersection point between the real RI of the core mode and SPP mode happened at 1.15 µm and intersection point between the real RI of the core and SPP modes happened at 1.15 µm and 1.3 µm, these wavelengths are called resonating wavelength. At that point, a deep steep peak in reasoning is seen, indicating the PCF core is where the most energy is being transferred to the SPP.

For the dispersion curve of RI (n = – 0.98), the core mode, coupling mode, and SPP mode are shown in blue, brown, and green color in Fig. 5. Core and SPP modes intersect at 1.15 µm and 1.3 µm wavelength.

Core-guided light is linked into the surface gold layer when the SPP and the core-guided modes phase-match. At that point, as shown in Fig. 6, the loss peak of core-guided modes is attained at a particular wavelength. Mostly, CL is used to describe the sensitivity of the corresponding structure.

Two methods (a) intensity or amplitude interrogation and (b) wavelength or spectral interrogation can be used to investigate the resonant wavelength shifts. The level of intended sensor sensitivity is determined by the perception of wavelength. Amplitude interrogation is more economical and easily implemented and hence no need for spectral manipulation. Also, its low sensing ability along with a small range of operations makes it (wavelength interrogation) a better choice. The WS of 29,264.8 nm/RIU, 39,952.05 nm/RIU, 40,124.11 nm/RIU, 40,132.06 nm/RIU, and 40,141.76 nm/RIU are observed, respectively, for RI values of – 0.96, – 0.97, – 0.98, – 0.99, – 1.

By using the AS method, the amplitude interrogation technique's complexity can be reduced. In Fig. 7, the AS is observed for the wavelength 1–1.7 µm for all the RI of COVID-19. At 1.15 µm wavelength, 48.54 RIU^{-1} of sensitivity is found for – 0.96 RI, maximum amplitude. For the RI of – 0.97, maximum amplitude sensitivity, 87 RIU^{-1} is observed at 1.15 µm. The greatest amplitude sensitivity for a RI of 0.98 is 77.69 RIU^{-1} at 1.55 µm. For the RI of – 0.99, its peak value of 43.77 RIU^{-1} is studied at the same wavelength (1.55 µm).

The cross-talk describes the quality of the photonic device by defining its ability to eliminate the undesirable polarized mode. In Fig. 8, for the RI of – 0.97, the maximum

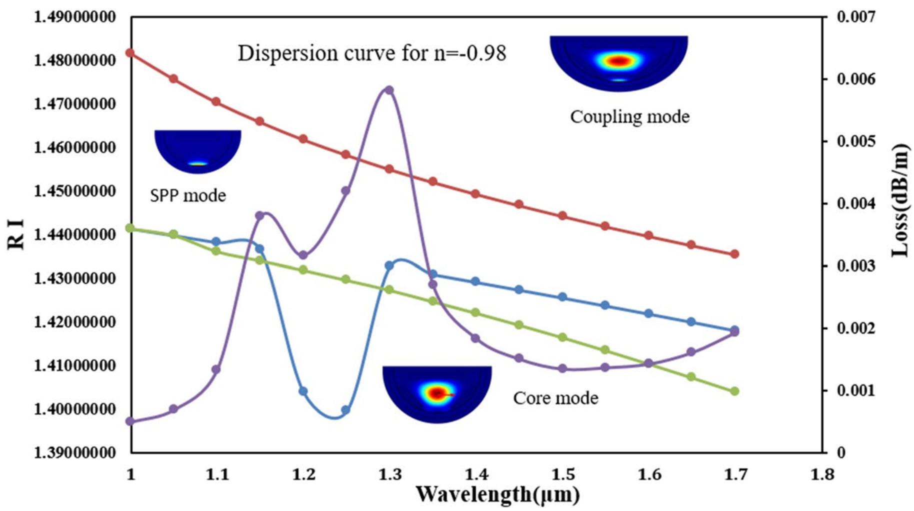

Fig. 5 Dispersion Curve for the proposed Biosensor for n = – 0.98

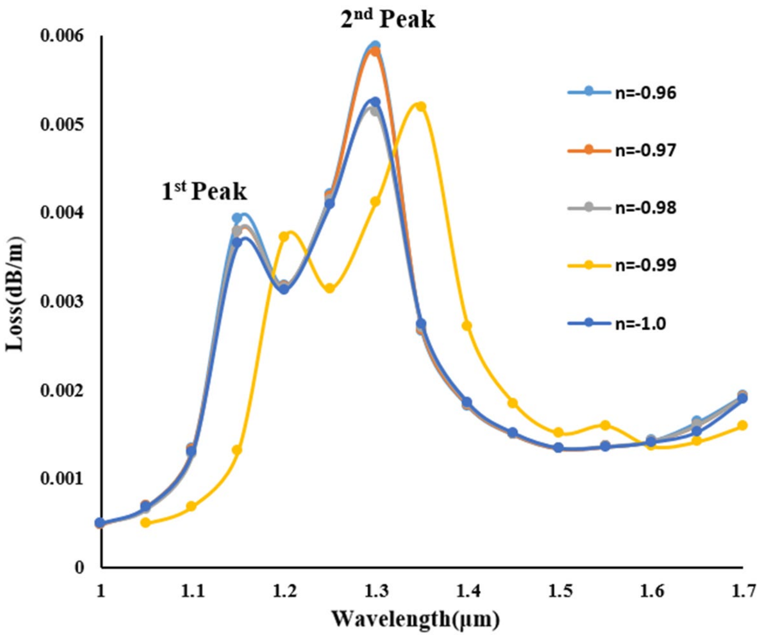

Fig. 6 The suggested sensor's loss curve with respect to wavelength

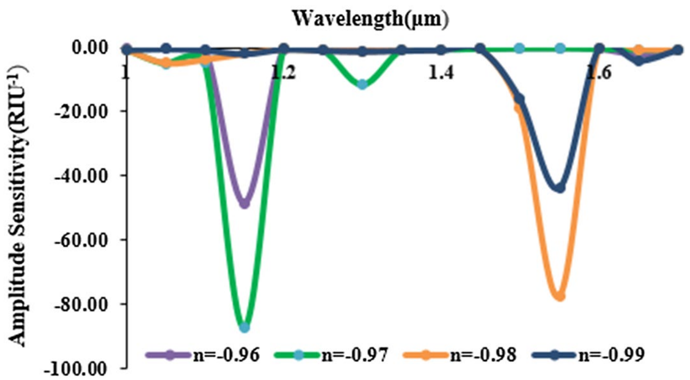

Fig. 7 AS curve as a function of wavelength

value of cross-talk is 7.56 dB at 1.15 μm wavelength. For − 0.98 the maximum cross talk is 7.74 dB at 1.55 μm wavelength. For the RI of − 0.96, the maximum cross-talk experienced is 4.24 dB for the wavelength 1.15 μm and also for the RI of − 0.99; the maximum cross-talk value is 3.8 dB at the same wavelength. These values indicate that very low cross talk (CT) is experienced for the designed sensor within the range of 1–1.7 μm wavelength. A viable choice for bio-sensing is the developed D-PCF with gold coating.

The insertion loss (IL) is another crucial parameter to gratify the characteristics of the PCF sensor. In Fig. 9, the lowest values of insertion loss for analyte − 0.97 to − 0.99

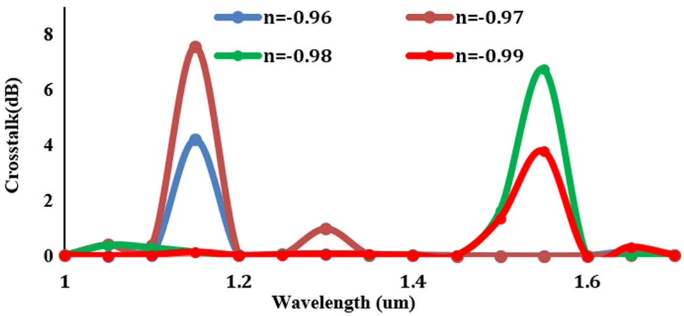

Fig. 8 Crosstalk of the proposed sensor as a function of wavelength

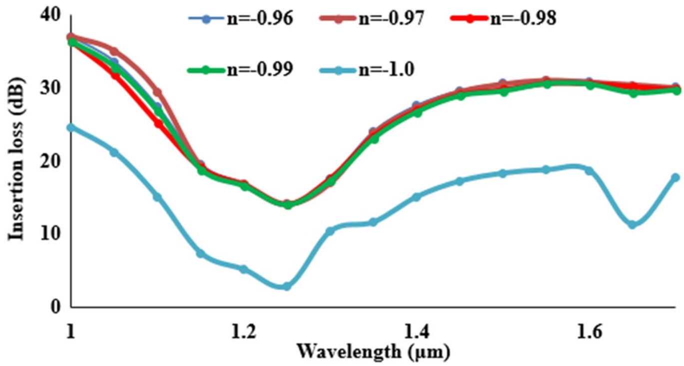

Fig. 9 Insertion loss of the proposed Corona sensor with respect to wavelength

lie within 14–15 dB for 1.25 μm wavelength. For the analyte of RI − 1, the minimum value is 2.91 dB at the same wavelength.

Simce obtained datasets are not in linear nature. A high polynomial fit curve shows the stability of the sensor. For the offered sensor, a high polynomial fit curve is obtained for the analyte − 0.96 to − 1 in Fig. 10. The R-square value is 0.97469 which specifies the high linearity. It is expected that such high linear characteristics can be used for corona testing. Table 4 exhibits the performance of the proposed sensor for corona detection. The performance comparison between the proposed PCF sensor and the previously reported PCF sensors has been shown in Table 5. It is visualized that the proposed sensor indicates better performance compare to recently reported sensors.

5 Fabrication possibility and discussion

Nowadays, the fabrication and drawing techniques of Photonic sensors are well developed. The D-shaped biosensor can be fabricated through the common stack-and-draw method (Knight et al. 1998). It is also explained in the article (Chen et al. 2016). The gold layer can be deposited on the surface of a D-shaped photonic sensor by applying deposition techniques like chemical vapor deposition (CVD), and splash technology (Peng et al. 2015; An

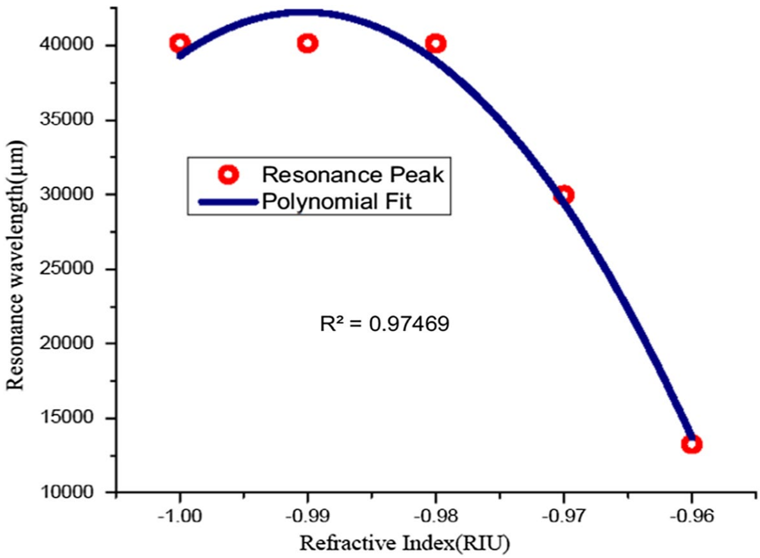

Fig. 10 The resonance wavelength curve with the polynomial fit and R-square value

Table 4 The described sensor's performance utilization for corona detection

RI	Peak loss (dB/cm)	Wavelength sensitivity (nm/RIV)	Cross talk (dB)	Insertion loss
−0.96	0.5864	29,264.8	4.24	14.19
−0.97	0.5799	39,952.05	7.56	14.11
−0.98	0.5134	40,124.11	7.74	14.04
−0.99	0.518	40,132.06	3.8	13.99
−1	0.523	40,141.76	5.24	2.91

Table 5 Performance comparison between the proposed PCF sensor and the previously reported PCF sensors

References	Structure	Birefringence	Wavelength sensitivity (nm/RIU)	Peak loss
Liu et al. (2018)	Dual D-shape PCF	–	14,660	17
Liu et al. (2018)	Single-layer coating PCF	–	15,180	110
Islam et al. (2019)	Exposed-core localized biosensor	–	34,000	0.79
Lu et al. (2018)	D-shaped PCF sensor	–	3340	140
Current work	D shape SPR-based structure	–	40,141.76	0.6

et al. 2014). It can also easily be fabricated by recent technology like sol–gel drilling and extrusion methods (Mamtaz et al. 2020; Paul et al. 2019, 2020; Hasan et al. 2022).

The quick detection of the new Coronavirus is demonstrated using a very sensitive D-shaped gold-coated SPR biosensor (COVID-19). The created SPR-based biosensor uses less time and provides a precise COVID-19 viral early-stage diagnosis. The suggested biosensor is used to identify cells that have been contaminated with the infectious bronchitis virus, or IBV, which is a member of the COVID19 family. The investigation procedure looks at some crucial optical factors, such as insertion loss, cross talk, and wavelength and amplitude sensitivity. Wavelength sensitivity is noted for refractive indices of – 0.96 , – 0.97, – 0.98, – 0.99, and 1 at 29,264.8 nm/RIU, 39,952.05 nm/RIU, 40,124.11 nm/RIU, 40,132.06 nm/RIU, and 40,141.76 nm/RIU, respectively.

Maximum amplitude sensitivity is determined to be 48.54 RIU^{-1}, 87 RIU^{-1} at 1.15 m, and 77.69 RIU^{-1}, 43.77 RIU^{-1} at 1.55 µm for RIs of 0.96, 0.97, 0.98, and 0.99. Moreover, the developed sensor exhibits very low cross talk (CT) in the 1 µm to 1.7 µm wavelength region. Another important element for enhancing the PCF sensor's features is the insertion loss (IL). The minimum result for the analyte with a RI of – 1 is 2.91 dB at the same wavelength (1.25 µm). A straightforward design compromises the proposed biosensor, which coats the gold-plasmonic substance and uses an external sensing method. The resonance wavelength sensitivity experimental findings and theoretical findings are closely connected. The suggested D-shaped model with gold coating is simple and inexpensive, and it could be employed for biochemical detection.

6 Conclusion

The detection of coronavirus utilizing its RI has been proposed and studied using a novel D-shaped PCF-based SPR biosensor. The proposed biosensor's computational domain has been handled by the FEM method, and in order to measure sensor performance, the most suitable plasmonic material—gold is externally deposited to reduce fabrication complexity and improve sensitivity. The suggested corona biosensor shows maximum AS of 100 RIU^{-1} and WS of 40,141 nm/RIU. Other optical parameters such as dispersion loss, confinement loss, cross-talk value, and insertion loss are also investigated for the wavelength region 1–1.7 µm. Since the suggested sensor is easy to fabricate by applying Draw and Stack technique. Due to its simple design and auspicious result, it can be noted that this sensor must be a good candidate in this COVID-19 pandemic and it must be a stair for the other sensor prepared for the detection of the coronavirus in the future.

Author contributions Conceptualization, Data curation, Formal analysis, Investigation, Methodology, TP Funding acquisition, SMI; Project administration, TP, SMI; Resources, Software, AMB; KAJA; Supervision, SMI; Validation, AMB; KAJA; Visualization, Writing—original draft, Writing—review editing, TP; SMI, KAJA; AMB.

Funding This study was supported by Researchers Supporting Project number (RSP2023R100), King Saud University, Riyadh, Saudi Arabia.

Availability of data and materials For any reasonable requests, get in touch with the corresponding author.

Code availability For any reasonable requests, get in touch with the corresponding author.

Declarations

Conflict of interest The authors declare no conflict of interest.

Ethical approval Not applicable.

Consent to participate Not applicable.

Consent to publish Not applicable.

References

Ahmadivand, A., Gerislioglu, B., Ramezani, Z., Kaushik, A., Manickam, P., Ghoreishi, S.A.: Femtomolar-level detection of SARS-CoV-2 spike proteins using toroidal plasmonic metasensors. arXiv preprint arXiv:2006.08536 (2020)

Ahmed, K., Ahmed, F., Roy, S., Paul, B.K., Aktar, M.N., Vigneswaran, D., Islam, M.S.: Refractive index-based blood components sensing in terahertz spectrum. IEEE Sens. J. **19**(9), 3368–3375 (2019)

Akib, T.B.A., Mou, S.F., Rahman, M.M., Rana, M.M., Islam, M.R., Mehedi, I.M., Mahmud, M.P., Kouzani, A.Z.: Design and numerical analysis of a graphene-coated SPR biosensor for rapid detection of the novel coronavirus. Sensors **21**(10), 3491 (2021)

An, G., Li, S., Qin, W., Zhang, W., Fan, Z., Bao, Y.: High-sensitivity refractive index sensor based on D-shaped photonic crystal fiber with rectangular lattice and nanoscale gold film. Plasmonics **9**, 1355–1360 (2014)

Astuti, I.: Severe acute respiratory syndrome coronavirus 2 (SARS-CoV-2): an overview of viral structure and host response. Diabetes Metab. Syndr. Clin. Res. Rev. **14**(4), 407–412 (2020)

Ayyanar, N., Raja, G.T., Sharma, M., Kumar, D.S.: Photonic crystal fiber-based refractive index sensor for early detection of cancer. IEEE Sens. J. **18**(17), 7093–7099 (2018)

Chen, Y., Xie, Q., Li, X., Zhou, H., Hong, X., Geng, Y.: Experimental realization of D-shaped photonic crystal fiber SPR sensor. J. Phys. D Appl. Phys. **50**(2), 025101 (2016)

Chen, Z.H., Li, Y.J., Wang, X.J., Ye, Y.F., Wu, B.L., Zhang, Y., Xuan, W.L., Bao, J.F., Deng, X.Y.: Chest CT of COVID-19 in patients with a negative first RT-PCR test: Comparison with patients with a positive first RT-PCR test. Medicine **99**(26), e20837 (2020)

Cui, D., Chen, X., Wang, Y.: Detection of SARS-CoV Antigen via SPR analytical systems with reference, p. 169. Pier Andrea Serra (2010)

Das, C.M., Guo, Y., Yang, G., Kang, L., Xu, G., Ho, H.P., Yong, K.T.: Gold nanorod assisted enhanced plasmonic detection scheme of COVID-19 SARS-CoV-2 spike protein. Adv. Theory Simul. **3**(11), 2000185 (2020)

Djaileb, A., Charron, B., Jodaylami, M.H., Thibault, V., Coutu, J., Stevenson, K., Forest, S., Live, L.S., Boudreau, D., Pelletier, J.N. and Masson, J.F.: A rapid and quantitative serum test for SARS-CoV-2 antibodies with portable surface plasmon resonance sensing. (2020)

Gheblawi, M., Wang, K., Viveiros, A., Nguyen, Q., Zhong, J.C., Turner, A.J., Raizada, M.K., Grant, M.B., Oudit, G.Y.: Angiotensin-converting enzyme 2: SARS-CoV-2 receptor and regulator of the renin-angiotensin system: celebrating the 20th anniversary of the discovery of ACE2. Circ. Res. **126**(10), 1456–1474 (2020)

Guo, Y., Li, J., Li, S., Zhang, S., Liu, Y.: Broadband single-polarization filter of D-shaped photonic crystal fiber with a micro-opening based on surface plasmon resonance. Appl. Opt. **57**(27), 8016–8022 (2018)

Hasan, M.M., Abdulrazak, L.F., Paul, B.K., Al-Zahrani, F.A., Ahmed, K.: Novel shaped solid-core photonic crystal fiber for the numerical study of nonlinear optical properties. Opt. Quantum Electron. **54**(3), 139 (2022)

Hossain, M.N., Tanvir, J., Aktar, M.N., Ahmed, K.: Design of a fuel adulteration detector sensor based on surface plasmon resonance. Opt. Quantum Electron. **55**(1), 61 (2023)

Islam, M.S., Sultana, J., Rifat, A.A., Ahmed, R., Dinovitser, A., Ng, B.W.H., Ebendorff-Heidepriem, H., Abbott, D.: Dual-polarized highly sensitive plasmonic sensor in the visible to near-IR spectrum. Opt. Express **26**(23), 30347–30361 (2018)

Islam, M.S., Islam, M.R., Sultana, J., Dinovitser, A., Ng, B.W.H., Abbott, D.: Exposed-core localized surface plasmon resonance biosensor. JOSA B **36**(8), 2306–2311 (2019)

Knight, J.C., Birks, T.A., Cregan, R.F., Russell, P.S.J., De Sandro, J.P.: Large mode area photonic crystal fibre. Electron. Lett. **34**(13), 1347–1348 (1998)

Korevaar, D.A., Kootte, R.S., Smits, L.P., van den Aardweg, J.G., Bonta, P.I., Schinkel, J., Vigeveno, R.M., van den Berk, I.A., Scheerder, M.J., Lemkes, B.A., Goorhuis, A.: Added value of chest computed tomography in suspected COVID-19: an analysis of 239 patients. Eur. Respir. J. **56**(2), 2001377 (2020)

Krüttgen, A., Cornelissen, C.G., Dreher, M., Hornef, M.W., Imöhl, M., Kleines, M.: Comparison of the SARS-CoV-2 Rapid antigen test to the real star Sars-CoV-2 RT PCR kit. J. Virol. Methods **288**, 114024 (2021)

Kuppuswamy, S., Swain, K., Nayak, S., Palai, G.: Computation of refractive indices of corona viruses through reverse calculation. Curr. Opt. Photonics **4**(6), 566–570 (2020)
Li, M., Peng, L., Zhou, G., Li, B., Hou, Z., Xia, C.: Design of photonic crystal fiber filter with narrow width and single-polarization based on surface plasmon resonance. IEEE Photonics J. **9**(3), 1–8 (2017)
Liu, Q., Li, S., Li, J., Dou, C., Wang, X., Wang, G., Shi, M.: Tunable fiber polarization filter by filling different index liquids and gold wire into photonic crystal fiber. J. Lightwave Technol. **34**(10), 2484–2490 (2016)
Liu, C., Su, W., Liu, Q., Lu, X., Wang, F., Sun, T., Chu, P.K.: Symmetrical dual D-shape photonic crystal fibers for surface plasmon resonance sensing. Opt. Express **26**(7), 9039–9049 (2018)
Liu, M., Yang, X., Shum, P., Yuan, H.: High-sensitivity birefringent and single-layer coating photonic crystal fiber biosensor based on surface plasmon resonance. Appl. Opt. **57**(8), 1883–1886 (2018)
Liu, C., Wang, J., Wang, F., Su, W., Yang, L., Lv, J., Fu, G., Li, X., Liu, Q., Sun, T., Chu, P.K.: Surface plasmon resonance (SPR) infrared sensor based on D-shape photonic crystal fibers with ITO coatings. Opt. Commun. **464**, 125496 (2020)
Lu, J., Li, Y., Han, Y., Liu, Y., Gao, J.: D-shaped photonic crystal fiber plasmonic refractive index sensor based on gold grating. Appl. Opt. **57**(19), 5268–5272 (2018)
Mak, G.C., Cheng, P.K., Lau, S.S., Wong, K.K., Lau, C.S., Lam, E.T., Chan, R.C., Tsang, D.N.: Evaluation of rapid antigen test for detection of SARS-CoV-2 virus. J. Clin. Virol. **129**, 104500 (2020)
Mamtaz, R., Ahmed, K., Paul, B.K., Mollah, M.A., Aktar, M.N., Uddin, M.S., Dhasarathan, V.: Design and FEM analysis of pentagonal photonic crystal fiber for highly non-linear applications. Opt. Quantum Electron. **52**, 1–13 (2020)
Mollah, M.A., Razzak, S.A., Paul, A.K., Hasan, M.R.: Microstructure optical fiber based plasmonic refractive index sensor. Sens. Bio-Sens. Res. **24**, 100286 (2019)
Mollah, M.A., Usha, R.J., Tasnim, S., Ahmed, K.: Detection of cancer affected cell using Sagnac interferometer based photonic crystal fiber refractive index sensor. Opt. Quantum Electron. **52**, 1–12 (2020)
Mollah, M.A., Habib, M.S., Habib, M.S.: Novel hollow-core asymmetric conjoined-tube anti-resonant fiber for low-loss THz wave guidance. OSA Contin. **3**(5), 1169–1176 (2020)
Momota, M.R., Hasan, M.R.: Hollow-core silver coated photonic crystal fiber plasmonic sensor. Opt. Mater. **76**, 287–294 (2018)
Paul, B.K., Ahmed, K., Vigneswaran, D., Sen, S., Islam, M.S.: Quasi photonic crystal fiber for chemical sensing purpose in the terahertz regime: design and analysis. Opt. Quantum Electron. **51**, 1–12 (2019)
Paul, B.K., Ahmed, K., Aktar, M.N.: Carbon disulphide (CS 2) enriched photonic crystal fiber for nonlinear application: a FEM scheme. Opt. Quantum Electron. **52**, 1–13 (2020)
Peng, L., Shi, F., Zhou, G., Ge, S., Hou, Z., Xia, C.: A surface plasmon biosensor based on a D-shaped microstructured optical fiber with rectangular lattice. IEEE Photonics J. **7**(5), 1–9 (2015)
Qin, W., Li, S., Yao, Y., Xin, X., Xue, J.: Analyte-filled core self-calibration microstructured optical fiber based plasmonic sensor for detecting high refractive index aqueous analyte. Opt. Lasers Eng. **58**, 1–8 (2014)
Shafkat, A.: Analysis of a gold coated plasmonic sensor based on a duplex core photonic crystal fiber. Sens. Bio-Sens. Res. **28**, 100324 (2020)
Sharan, P., Bharadwaj, S.M., Gudagunti, F.D. and Deshmukh, P.: January. Design and modelling of photonic sensor for cancer cell detection. In 2014 International Conference on the IMpact of E-Technology on US (IMPETUS), pp. 20–24. IEEE (2014)
Shirato, K., Semba, S., El-Kafrawy, S.A., Hassan, A.M., Tolah, A.M., Takayama, I., Kageyama, T., Notomi, T., Kamitani, W., Matsuyama, S., Azhar, E.I.: Development of fluorescent reverse transcription loop-mediated isothermal amplification (RT-LAMP) using quenching probes for the detection of the Middle East respiratory syndrome coronavirus. J. Virol. Methods **258**, 41–48 (2018)
Sorathiya, V., Patel, S.K., Ahmed, K., Taya, S.A., Das, S., Murali Krishna, C.: Multi-layered graphene silica-metasurface based infrared polarizer structure. Opt. Quantum Electron. **54**(4), 254 (2022)
Srinivasan, K., Radhakrishnan, G., Mohammadd, N., Amin, R., Ahmed, K., Bui, F.M., Ibrahim, S.M., Alsalem, K.A.J.: Ultra-high negative dispersion compensating circular-shaped PCF with highly birefringent and nonlinear characteristics for optical applications. Opt. Quantum Electron. **54**(12), 834 (2022)
Tanvir, J., Mitu, S.A., Tahhan, S.R., Ahmed, K., Bui, F.M., Patel, S.K., Al-Zahrani, F.A.: Terahertz spectroscopic based bending effect inspection on hollow-core anti-resonant fiber. Opt. Quantum Electron. **55**(4), 305 (2023)
Vigneswaran, D., Ayyanar, N., Sharma, M., Sumathi, M., Rajan, M., Porsezian, K.: Salinity sensor using photonic crystal fiber. Sens.actuators A Phys. **269**, 22–28 (2018)
Vigneswaran, D., Rajan, M.S.M., Biswas, B., Grover, A., Ahmed, K., Paul, B.K.: Numerical investigation of spiral photonic crystal fiber (S-PCF) with supporting high order OAM modes propagation for space division multiplexing applications. Opt. Quantum Electron. **53**, 1–11 (2021)

Yan, C., Cui, J., Huang, L., Du, B., Chen, L., Xue, G., Li, S., Zhang, W., Zhao, L., Sun, Y., Yao, H.: Rapid and visual detection of 2019 novel coronavirus (SARS-CoV-2) by a reverse transcription loop-mediated isothermal amplification assay. Clin. Microbiol. Infect. **26**(6), 773–779 (2020)

Yang, X., Lu, Y., Liu, B., Yao, J.: Design of a tunable single-polarization photonic crystal fiber filter with silver-coated and liquid-filled air holes. IEEE Photonics J. **9**(4), 1–8 (2017)

Zakaria, R., Zainuddin, N.A.A.M., Ahmad Fahri, M.A.S., Kamkar, A., Al Zahrani, F.A., Patel, S.K., Ahmed, K.: Exploration of multi-metallic thin layer/MgF_2 in side-polished optical fiber as long-range surface plasmons (LRSPs) alcohol sensor. Opt. Quantum Electron. **54**(4), 221 (2022)